Journal of Nuclear Medicine, published on February 24, 2022 as doi:10.2967/jnumed.121.263555

Cardiac Fibroblast Activation in Patients Early After Acute Myocardial Infarction: Integration with Magnetic Resonance Tissue Characterization and Subsequent Functional Outcome

Johanna Diekmann, MD[1]*; Tobias Koenig, MD[2]*; James T. Thackeray; PhD[1]; Thorsten Derlin, MD[1]; Christoph Czerner[1], MD[2]; Jonas Neuser, MD[2]; Tobias L. Ross, PhD[1]; Andreas Schäfer[2], MD; Jochen Tillmanns, MD[2]; Johann Bauersachs, MD[2]*; Frank M. Bengel, MD[1]*

[1] Department of Nuclear Medicine, Hannover Medical School, Hannover, Germany

[2] Department of Cardiology and Angiology, Hannover Medical School, Hannover, Germany

* contributed equally

Short title: ^{68}Ga-FAPI PET, CMR and Outcome after AMI

Word count (abstract): 297

Word count (manuscript text): 5132

Address for correspondence:

Frank M. Bengel, MD, FAHA

Department of Nuclear Medicine, Hannover Medical School

Carl-Neuberg-Str. 1

30625 Hannover, Germany

Telephone: +49 511 532 2577

E-Mail: bengel.frank@mh-hannover.de

Johanna Diekmann, MD

Department of Nuclear Medicine, Hannover Medical School

Carl-Neuberg-Str. 1

30625 Hannover, Germany

Telephone: +49 511 532 2577

E-Mail: diekmann.johanna@mh-hannover.de

ABSTRACT

Background and Rationale

After acute myocardial infarction (AMI), fibroblast activation protein (FAP) upregulation exceeds the infarct region. We sought further insights into the physiologic relevance by correlating FAP-targeted PET with tissue characteristics from cardiac magnetic resonance (CMR) and functional outcome.

Methods

Thirty-five patients underwent CMR, perfusion SPECT, and ^{68}Ga-FAPI-46 PET/CT within 11 days after AMI. Infarct size was determined from SPECT by comparison to reference database. For PET, regional standardized uptake values (SUV) and isocontour volumes-of-interest (VOI) determined the extent of cardiac FAP upregulation (FAP-volume). CMR yielded functional parameters, area of injury (late gadolinium enhancement, LGE) and T1/T2 mapping. Follow-up was available from echocardiography or CMR after 139.5 (IQR 80.5-188.25) days (n=14).

Results

The area of FAP-upregulation was significantly larger than SPECT perfusion defect size (58±15 vs. 23±17%, $p<0.001$) and infarct area by LGE (28±11%, $p<0.001$). FAP-volume significantly correlated with CMR parameters at baseline (all $p<0.001$): infarct area ($r=0.58$), left ventricular (LV) mass ($r=0.69$), endsystolic ($r=0.62$) and enddiastolic volume ($r=0.57$). Segmental analysis revealed FAP-upregulation in 308/496 myocardial segments (62%). Significant LGE was found in only 56% of FAP-positive segments, elevated T1 in 74%, and elevated T2 in 68%. 14% (44/308) of FAP-positive segments exhibited neither prolonged T1 or T2 nor significant LGE. Of note, FAP-volume correlated only weakly with simultaneously measured left ventricular ejection fraction (LVEF) at baseline ($r=-0.32$, $p=0.07$), whereas there was a significant inverse correlation with LVEF obtained at later follow-up ($r=-0.58$, $p=0.007$).

Conclusion

Early after AMI and reperfusion therapy, activation of fibroblasts markedly exceeds the hypoperfused infarct region and involves non-infarcted myocardium. The ^{68}Ga-FAPI PET signal does not match regional myocardial tissue characteristics as defined by CMR, but it is predictive of the evolution of ventricular dysfunction. FAP-targeted imaging may provide a novel biomarker of left ventricular remodeling that is complementary to existing techniques.

KEY WORDS:

Myocardial infarction, fibroblast activation protein, positron emission tomography, left ventricular remodeling

INTRODUCTION

Fibrotic tissue remodeling after injury leads to functional impairment and adverse outcome of the affected structure or organ. In cardiac disease, myocardial fibrosis contributes to the development and progression of heart failure. Recent evidence has highlighted molecular pathways that activate quiescent cardiac fibroblasts, which have emerged as attractive therapeutic targets to support cardiac repair and mitigate loss of function (*1-4*).

Acute myocardial infarction (AMI) is an important contributor to the development of heart failure (*5*). Here, an immediate and organized inflammatory immune reaction triggers the activation of quiescent fibroblasts (*6,7*). Activated myofibroblasts migrate to injured tissue and contribute to fibrotic scar formation. Sufficient scar is required for adequate repair, but excessive pro-fibrotic response and involvement of remote myocardium support adverse ventricular remodeling, culminating in progressive contractile dysfunction (*6,8*). Accordingly, while fibrosis has emerged as a potential therapeutic target, its double-edged nature after AMI likely requires a personalized approach for medical decision-making. Non-invasive, quantitative, fibrosis-targeted imaging may be instrumental for this purpose.

Fibroblast activation protein (FAP) is a membrane-bound serine protease (*2,9*) highly expressed by activated myofibroblasts. Recently, several FAP inhibitors (FAPI) have been introduced for targeted positron emission tomography (PET). Initially, ^{68}Ga-FAPI PET was employed for imaging of various tumors (*10*), but retrospective analysis of oncologic cohorts established an association between FAP signal and cardiac risk factors, including arterial hypertension and diabetes mellitus (*11*). Increased cardiac signal has also been reported after chemotherapy or chest radiotherapy (*12*). Recently, experimental studies supported the feasibility of ^{68}Ga-FAPI PET to identify fibroblast activation in animal models of AMI (*13,14*). Additionally, clinical reports confirmed a strong ^{68}Ga-FAPI PET signal in patients with AMI, which frequently exceeded the nonviable infarct area (*15-17*). Whether this phenomenon is predictive of adverse

functional outcome, however, remains unknown. Likewise, the relationship between ^{68}Ga-FAPI PET signal and cardiac magnetic resonance (CMR) tissue characteristics is not well defined. CMR identifies late gadolinium enhancement (LGE) in injured regions, and it provides extracellular volume, native T1 and T2 relaxation times as measures of tissue fibrosis (T1) and edema (T2) throughout the entire myocardium (*18*). In contrast to ^{68}Ga-FAPI PET, which identifies a cellular signal from activated myofibroblasts, these CMR-derived parameters mostly reflect extracellular tissue composition.

We hypothesized that ^{68}Ga-FAPI PET reflects a myocardial signal early after AMI that is not identical to CMR-derived tissue characteristics and that predicts later development of ventricular dysfunction. Our hypothesis was tested in a cohort of AMI patients that underwent multi-parametric, multi-modality noninvasive cardiac imaging early after standard-of-care reperfusion therapy.

MATERIALS AND METHODS

Study Design and Participants

This retrospective single-center study included 35 consecutive patients (30 males, 5 females; 57±11yrs) that had undergone clinical resting myocardial perfusion single-photon emission computed tomography (SPECT), FAP-targeted PET with ^{68}Ga-FAPI-46 and CMR within 11d after reperfusion therapy for AMI at Hannover Medical School (MHH). All subjects had been treated by percutaneous coronary intervention and stenting within 4±3hrs of symptom onset and received dual anti-platelet therapy. All had ST-segment elevation, absence of a prior history of AMI or coronary intervention or other cardiac procedures, success of reperfusion immediately after angioplasty, absence of systemic immunologic or infectious or pro-fibrotic disease, and availability of complete imaging datasets, clinical records and laboratory parameters. Clinical characteristics

and medication at the time of imaging are summarized in table 1. Routinely recorded laboratory values, as determined by standard MHH clinical procedures, included peak creatine kinase as a marker of myocardial injury, and C-reactive protein and leukocyte count as markers of systemic inflammatory response. The institutional review board approved the project (#9553_BO_K_2021) and all subjects signed a written consent form.

Radionuclide Imaging

At 5.0±1.5d after AMI (median 5.0; range, 3-8d), resting myocardial perfusion SPECT was obtained to determine success of reperfusion, using 388±32 MBq of ^{99m}Tc-tetrofosmin and a dedicated cardiac camera (GE Discovery 530c, GE Healthcare, Waukesha, WI, USA). Infarct size was determined using commercially available software for polar map generation (4DM, Invia, Ann Arbor, MI, USA) and a local normal database for comparison.

FAP-targeted PET was conducted at 7.5±1.3d (range, 5-11d) using the specific ligand, ^{68}Ga-FAPI-46, which was synthesized in house by good manufacturing practice as previously described (*19*) and used clinically according to §13.2b of the German Pharmaceuticals Act, for determination of myocardial injury. Static PET images were acquired for 20min using a Biograph mCT 128 PET/CT system (Siemens, Knoxville, TN, USA), beginning 60min after intravenous injection of 114±22 MBq of ^{68}Ga-FAPI-46. Low-dose computed tomography (CT) was used for attenuation correction. Images were iteratively reconstructed, using time-of-flight and point-spread function information (True X, Siemens). Peak and mean standardized uptake values (SUV) were obtained for infarct, remote myocardium, blood pool (left atrium) and other organs using volumes-of-interest (VOI) of 1 cm^3 and commercial software (syngo.via; V50B, Siemens Healthcare). Cardiac FAP volume was determined by isocontour VOI including all voxels above an individual threshold (blood pool SUVmean+2standard deviations (SD)). We set this threshold due to lack of an established alternative standard. Additionally, area of FAP upregulation was calculated by polar

map analysis, using the same threshold, as previously described (*15*). Mean segmental SUV was calculated using the AHA 17 segments model and polar maps.

Cardiac Magnetic Resonance Imaging

CMR was performed using a 1.5T scanner (Magnetom Avanto, Siemens) in 33/35 patients (94%) at 4±2d after AMI (median 4; range, 2-10d). Cine images were obtained using a balanced steady state free precession sequence (True FISP). Parametric T1 and T2 maps were acquired in three short-axis slices (basal, midventricular and apical left ventricle) covering 16 segments (available for 31 patients). T1 mapping was performed using the modified Look-Locker (MOLLI) sequence before (native) and after administration of contrast agent. Quantitative balanced steady-state free procession-based T2 maps (True FISP) were acquired in corresponding short-axis slices. Upper threshold of normal T1 was defined as 1023ms and T2 as 60ms according to our clinical standard (*20,21*). LGE was imaged by phase-sensitive inversion recovery (PSIR) sequences, 10-15 min after bolus injection of 0.15 mmol/kg gadolinium-DTPA (Gadobutrol, Bayer Healthcare). Extracellular volume fraction (ECV) was calculated by measurement of myocardial and blood T1 relaxation times before and after administration of contrast and using hematocrit value. Global analysis included determination of LVEF, volumes, mass, extent of LGE and microvascular obstruction (MO). Segmental analysis included wall thickening, native T1 and T2 relaxation times, and ECV, using the 16-segments model. cvi42 software (Circle Cardiovascular Imaging, Calgary, Canada) was used.

Follow-up Left Ventricular Function

In 14/35 patients (40%), follow-up LVEF was available from standardized in-house echocardiography (biplane Simpson method, n=12) or repeat cine CMR (n=2), at a mean of 133±63d (median140; range 42-214d) after AMI.

Statistical Analysis

Statistical analyses were performed using SPSS version 27 and Graphpad Prism version 9. Categorical variables are presented with absolute and relative frequencies. For quantitative continuous variables, testing of Gaussian distribution was performed using Shapiro-Wilk tests. For data with Gaussian distribution, paired Student's t-tests or one-way analysis of variance (ANOVA) with Tukey multiple comparison tests were used respectively. Non-parametric unpaired data were analyzed with Mann-Whitney-U-tests. Pearson correlation coefficients were calculated for bivariate correlation analyses. All statistical analyses were performed two-sided and a p-value <0.05 indicated statistical significance.

RESULTS

FAP Signal Exceeds the Infarct Region and Correlates with Blood Markers of Tissue Damage and Inflammation

Perfusion defect size in SPECT was 23±17% of left ventricle (LV), ranging from 0-55%. In 7/35 (20.0%) patients, complete reperfusion was documented by absence of significant perfusion defect. Myocardial injury as measured by LGE volume comprised 40±19ml or 28±11% of LV (range 1-49%), and correlated with perfusion defect size (r=0.646, p<0.001). Other CMR-derived global parameters are summarized in table 2.

^{68}Ga-FAPI PET showed significantly elevated signal in the territory of the culprit infarct vessel (SUV_{peak} 6.4±1.5) in all patients. PET imaging ranged from 5-11 days after AMI and no significant relationship between myocardial FAP volume and time after AMI was detected within this interval (Spearman rho: r=0.056, p=0.750). Consistent with prior reports, the majority of patients showed markedly larger areas of elevated FAP signal when compared to either the SPECT perfusion defect (58±15% vs 23±17%, p<0.001) or the extent of myocardial injury

measured by LGE (28±11%, p<0.001, figure 1, patient example figure 2). Even among the 7 patients with complete reperfusion and absence of SPECT perfusion defect, an elevated FAP signal was consistently detected in the affected coronary territory (figure 3). Low amounts of LGE were detected in patients without residual SPECT perfusion defect, however LGE was less prominent than in other patients (13.7±9.8 vs. 31.5±8.8%, P<0.001) and FAP signal was significantly larger (54.7±19.4%, P<0.001). Only 3/35 patients had a difference between FAP area and infarct size of <15%, all of whom exhibited large perfusion defects (figure 4). Area of FAP-upregulation correlated with perfusion defect size (r=0.407, p=0.015) and LGE (r=0.344, p=0.050), suggesting that larger infarcts also lead to larger amounts of replacement fibrosis. Of note, however, mismatch area between FAP-area and perfusion defect size as a marker of viable myocardium with activated fibroblasts, inversely correlated with perfusion defect size (r=-0.622, p<0.001). The specific number of days after AMI at which imaging was performed in this study did not have a significant effect on differences between CMR, perfusion and ^{68}Ga-FAPI PET patterns (data not shown). Further results of ^{68}Ga-FAPI PET are summarized in table 3. Only two patients presented with small amounts of MO (<5%). With 69% (24/35) LAD was the most frequent culprit vessel (table 1). Here, FAP area was larger when compared to other coronary territories (LAD 64.8±12.6 vs. LCX 41.0±13.8 vs. RCA 44.1±8.7, P(ANOVA)<0.001), but mismatch between FAP area and perfusion defect size did not show significant differences between coronary territories.

Of note, signal in remote myocardium and other regions (liver, spleen, bone marrow, lung) was low and did not correlate with infarct signal. Significant correlations were detected between FAP volume and CK max (r=0.42, p=0.012) as well as inflammatory markers (CRP max: r=0.43, p=0.010, WBC max: r=0.31, p=0.07). Diabetes mellitus was associated with a larger FAP volume (134±53 cm³ vs. 93±36 for patients without diabetes p=0.012), while other cardiovascular risk factors were not associated with FAP signal.

FAP Signal Does Not Match Regional CMR Tissue Characteristics Segmental Analysis

For segmental correlation with CMR, apex was excluded studies, leaving 16 segments per patient and a total of 496 segments (CMR T1 and T2 mapping available in 31 patients). Overall, segmental mean FAP signal correlated with LGE extent (r=0.660, p<0.001), T1 and T2 relaxation times (r=0.485, p<0.001 and r=0.475, p<0.001), extracellular volume (r=0.557, p<0.001). But there were marked differences when classifying segments as positive or negative for the respective tissue parameter (figure 5): 308/496 (64%) segments were classified as FAP-positive (FAP+), using blood pool SUV_{mean}+2SD as a threshold (*15*). Transmural LGE signal >25% was present in 172/308 segments (56%). Prolonged T1 relaxation time above 1023ms (*22*), a threshold indicative of tissue fibrosis, was present in 227/308 segments (74%). Prolonged T2 relaxation time longer than 60ms (*21*), consistent with edema, was present in 210/308 segments (68%). Of note, 44/308 (14%) FAP+ segments had normal T1 and T2 relaxation and no relevant LGE. This confirms that FAP-signal frequently extends beyond areas that are abnormal at CMR tissue characterization. Only few FAP- segments showed LGE or altered T1 and T2 relaxation times. In these segments, LGE most likely reflects chronic stages of (pre-existing) scar, potentially due to cardiovascular comorbidities. Furthermore, elevated signal in T1/T2 mapping in the absence of FAP signal may identify segments with edema but no fibroblast activity.

FAP Positive Segments Present with Impaired Contractility

Segmental SUV_{mean} (n=496 segments) showed a mild but significant inverse correlation with segmental wall thickening (r=-0.224, p<0.001). When comparing 3 subgroups of segments, normally perfused segments without FAP signal had significantly higher wall thickening when compared to normally perfused segments with elevated FAP signal, while wall thickening was lowest in hypoperfused segments, which all had elevated FAP signal (figure 6).

FAP Signal Correlates with Ventricular Geometry and Functional Outcome

At baseline, FAP volume significantly correlated with LV mass (r=0.69; p>0.001), end-diastolic (r=0.57; p>0.001) and end-systolic volume (r=0.62; p>0.001), and LGE volume (r=0.58; p>0.001). A trend to correlation was detected between FAP volume and initial LVEF (r=-0.32, p=0.07). Interestingly, FAP volume showed a stronger, significant correlation with LVEF at follow-up (r=-0.583, p=0.007; figure 7). Among patients with complete follow-up, those with at least one FAP-positive, but T1, T2 and LGE-negative segment (n=6) had a lower follow-up LVEF than those without such segments (n=6; 47±8% vs 57±3%, p=0.02). Overall, this suggests that a higher amount of activated fibroblasts early after AMI is associated with more severe LV dysfunction in the subsequent chronic stage after AMI.

DISCUSSION

In summary, our results confirm that regional upregulation of FAP by activated fibroblasts yields a very high contrast between injured infarct and peri-infarct region and unaffected remote myocardium, blood pool and surrounding structures. FAP-upregulation markedly exceeds the infarct region in patients early after AMI and standard-of-care reperfusion therapy. This is consistent with the notion that FAP upregulation plays a role not only in replacement fibrosis in the primary injured region, but also in reactive fibrosis that may compromise non-infarcted myocardium (*15,23*). Our observation of a link between extent of early FAP signal and LV dysfunction at later follow-up lends further support to this concept. Our results suggest that the FAPI signal is a multifactorial parameter, which integrates a variety of influencing factors in the commonly heterogeneous clinical setting of patients early after AMI. Yet, the association with functional outcome makes the parameter intriguing for further exploration.

Integrative multi-modal segmental analysis provides further insights into the relationship between fibroblast activation and extracellular tissue composition. Interestingly, the mismatch between FAP-area and perfusion defect size was larger when infarct size was smaller. Speculatively, larger amounts of myocardial salvage and reperfusion injury may contribute to this elevated FAP signal as a potential precursor of interstitial fibrosis. Future studies may provide further insights into these interrelations. While we found that FAP upregulation grossly correlated with CMR tissue parameters, there were relevant regional discordances. A significant fraction of FAP-positive segments not only exhibited absent LGE, but also lacked prolongation of T1 and T2 relaxation times on CMR. This finding is of particular interest because it suggests that results of ^{68}Ga-FAPI PET are not interchangeable with CMR tissue characteristics. Rather, ^{68}Ga-FAPI PET may add further, biologically distinct information. Currently, LGE imaging is well established for detection of focal, mostly replacement fibrosis following myocardial injury in ischemia, inflammation or cardiomyopathy. But cardiac pathologies including diffuse, mostly interstitial alterations such as fibrosis or edema, cannot be quantified adequately by LGE (*24*). For this purpose, CMR mapping techniques have been successfully designed, which quantitatively determine tissue relaxation times for T1 (prolonged e.g. in interstitial fibrosis and infiltration), and T2 (primarily reflecting water content and prolonged in edema and inflammation). These parameters are increasingly applied in the clinics (*25*) and provide information about the extent and composition of extracellular space. Myocardial fibrosis is commonly defined as an expansion of the cardiac interstitium by deposition of extracellular matrix proteins such as collagen. But modern concepts of the pathogenesis of fibrosis increasingly emphasize the role of cellular components, where there is a tight interplay between functionally diverse subsets of fibroblasts, extracellular matrix composition and regulation by the immune system (*26*). ^{68}Ga-FAPI PET identifies the cellular component of this process, by specifically visualizing the expression of FAP on activated myofibroblasts (*9,13,14*). Our results suggest that this pro-fibrotic cellular signal is abundant in the territory of the infarct vessel early after AMI, that it may be present in myocardial

segments that do not (yet) show elevated T1 relaxation as a measure of interstitial protein deposition, and in segments that do not (still) show elevated T2 as a measure of edema. Speculatively, elevated FAP signal is an early and abundant fibroblast response following reperfusion and its immediate inflammatory reaction. The cellular FAP signal may then precede the subsequent deposition of extracellular matrix that establishes overt fibrosis. Clearly, further work is needed to elucidate the relative time course of the cellular, PET-derived signal and the interstitial, CMR-derived signal, along with their importance for functional outcome and for guidance of therapeutic interventions. In this regard, it should be noted that PET with other, immune cell-targeted tracers, may also identify the cellular component of inflammation, for integration with fibrosis-targeted imaging (*27,28*).

Regional patterns in our AMI patients suggest that the area of FAP upregulation may be interlinked with the ischemic area at risk (AAR). Prior SPECT studies have shown feasibility of AAR assessment using perfusion imaging after radiotracer injection prior to and after reperfusion of AMI (*29*). Yet, this logistically demanding approach is not broadly feasible and has not been available in our setting. In CMR, AAR has been proposed to be estimated via quantity of edema in T2-weighted images, but preclinical histologic validation delivered partly inconclusive results on colocalization of edema and AAR(*30*). In our study, FAP signal partly colocalized with detected edema in T2 weighted images. Interestingly, the mismatch of FAP-area and perfusion defect size was larger when infarct size was smaller, suggesting a relationship with successful reperfusion. FAP+ segments also showed impaired wall thickening both in the infarct and in the border zone, where it may reflect regional postischemic stunning. And last, the detected correlation of FAP uptake with levels of CK suggest an association between amount of activated fibroblasts and ischemia/reperfusion ischemic injury. Ultimately, the relationship between area of fibroblast activation and AAR warrants further investigation. Inclusion of myocardial perfusion imaging after tracer injection prior to revascularization, or the addition of stress perfusion imaging for flow reserve measurements may be helpful in this regard in the future.

The long-term importance of imaging the myofibroblast component of pro-fibrotic activity will depend on its predictive value for subsequent LV remodeling and heart failure progression. Our results show that the area of fibroblast activation at the time of PET imaging was associated with the extent of injury and geometric features such as mass and volumes of the LV, while the relation with contractile function was less pronounced initially. This relationship, however, changed at follow-up in the chronic post-AMI stage, where a larger extent of FAP signal early after AMI was associated with more severe contractile dysfunction. Notably, we even observed lower mean follow-up LVEF in patients with FAP positive but CMR negative tissue signal early after AMI. This might be a first indicator supporting an independent relevance of myocardial FAP signal for functional outcome, however follow-up of LV function was only available in 14 patients. Larger prospective work will be needed to confirm these results.

We also observed a larger extent of myocardial fibroblast activation in a subgroup of patients with diabetes mellitus, while no differences were found analyzing other cardiovascular risk factors (age, gender, arterial hypertension, hyperlipidemia, smoking and obesity). This finding was independent of infarct size. In AMI, diabetes mellitus is associated with elevated long-term mortality (*31,32*). Also, it has been shown that patients with adult-onset diabetes may exhibit extensive perivascular, interstitial, and even replacement fibrosis, in the absence of hypertension or coronary artery disease (*33*). The molecular mechanisms responsible for the contribution of diabetes mellitus to cardiac fibrosis remain poorly understood (*34*). Whether a more pronounced fibroblast activation in response to ischemic hypoperfusion plays a role in the adverse outcome of diabetic patients is another hypothesis generated by our preliminary observation that should be tested in subsequent studies.

A strong FAP signal was measured in the affected region while signal from remote myocardium and other regions (liver, spleen, bone marrow, lungs) was much lower. This supports the feasibility of FAP-targeted imaging to guide anti-fibrotic therapeutic strategies. Importantly, it

also supports the feasibility of FAP-targeted therapies themselves, which may modulate and attenuate pro-fibrotic activity if administered precisely in suitable individuals and at the right time (*3*). In the future, molecular imaging using FAPI-ligands might help to understand mechanisms and select patients for individual treatment using advanced anti-fibrotic measures.

Some limitations of our work should be considered: The sample size was small and the analysis was retrospective, leading to even smaller samples for follow-up. No serial imaging was performed and the time course of the FAP signal after AMI remains incompletely defined. We chose to use a threshold for detection of FAP-positive myocardial areas due to absence of an established standard. It should be noted that this approach was pursued as a best possible approach in the absence of validated alternatives. Other measures such as the SUV or segmental analyses were threshold-independent and confirm the major conclusions of our work. Our work should be seen as hypothesis-generating for further studies, which may aim at identifying the optimal time point for imaging FAP expression in order to predict the progression of post-infarct remodeling most effectively. Further work may also focus on defining the incremental value of FAP-targeted imaging over standard clinical risk markers, CMR and other molecular targeted approaches such as imaging of the inflammatory response to injury (*35*). The outcome sample of this study was too small for meaningful multi-variate analyses. Finally, matching of PET and CMR results may not have been perfect because studies were obtained on separate camera systems on different days. We also cannot completely discount possible variation of imaging parameters over time in this study, although we sought to minimize effects by performing imaging on three consecutive days, where possible. PET signal was significantly elevated in the infarct region and in the peri-infarct region, where wall thickening was impaired as a consequence of ischemic injury. Partial volume effects were considered minor therefore and in the absence of established methods, no correction for partial volume effects was applied. In the future, hybrid PET-MR systems may offer simultaneous acquisition of CMR and PET parameters of myocardial repair after AMI (*36*).

CONCLUSION

Taken together, this work provides new insights into the regional pattern of fibroblast activation early after AMI. The area of elevated FAP signal reaches beyond the injured infarct region and may even involve regions without prolonged T1 or T2 relaxation as CMR markers of interstitial fibrosis, infiltration or edema. This suggests that the cell-based signal of fibroblast activation is distinct from CMR-derived interstitial characteristics, and may be complementary. Importantly, the early FAP signal was associated with a subsequent impairment of LV function, suggesting that it may be a predictor of adverse LV remodeling.

ACKNOWLEDGEMENTS

Funding:

Supported by the Deutsche Forschungsgemeinschaft (DFG, Clinical Research Unit KFO 311, JB, FMB and Clinician Scientist Program PRACTIS, JD), the Leducq Foundation (Transatlantic Network „Immunofib“, FMB, JTT, JD), and “REBIRTH – Research Center for Translational Regenerative Medicine” (State of Lower Saxony; JTT, JB, FMB)

Disclosures:

The authors have no relationships relevant to the contents of this paper to disclose. No potential conflicts of interest relevant to this article exist. Precursor for ^{68}Ga-FAPI-46 was kindly provided by Uwe Haberkorn, MD, University of Heidelberg.

KEY POINTS

Question:

Does myocardial fibroblast activation early after acute myocardial infarction (AMI) correlate with cardiac magnetic resonance (CMR) tissue characteristics, and is it predictive of subsequent development of ventricular dysfunction?

Pertinent Findings:

35 patients underwent ^{68}Ga-FAPI-46 PET and CMR within 11d after reperfusion therapy for (AMI). The region of fibroblast activation on ^{68}Ga-FAPI PET extended beyond the fibrotic scar. Also, there were segmental discrepancies between FAPI signal and T1 and T2 relaxation times from CMR. FAPI signal early after AMI correlated with reduced LVEF in the subsequent chronic stage.

Implications for Patient Care:

^{68}Ga-FAPI PET may be complementary to CMR and serve as an independent marker of the risk of adverse cardiac remodeling after AMI.

REFERENCES

1. Travers JG, Kamal FA, Robbins J, Yutzey KE, Blaxall BC. Cardiac Fibrosis: The Fibroblast Awakens. *Circ Res.* 2016;118:1021-1040.

2. Furtado MB, Nim HT, Boyd SE, Rosenthal NA. View from the heart: cardiac fibroblasts in development, scarring and regeneration. *Development.* 2016;143:387-397.

3. Aghajanian H, Kimura T, Rurik JG, et al. Targeting cardiac fibrosis with engineered T cells. *Nature.* 2019;573:430-433.

4. Gourdie RG, Dimmeler S, Kohl P. Novel therapeutic strategies targeting fibroblasts and fibrosis in heart disease. *Nat Rev Drug Discov.* 2016;15:620-638.

5. Conrad N, Judge A, Tran J, et al. Temporal trends and patterns in heart failure incidence: a population-based study of 4 million individuals. *Lancet.* 2018;391:572-580.

6. Prabhu SD, Frangogiannis NG. The Biological Basis for Cardiac Repair After Myocardial Infarction: From Inflammation to Fibrosis. *Circ Res.* 2016;119:91-112.

7. Lafuse WP, Wozniak DJ, Rajaram MVS. Role of Cardiac Macrophages on Cardiac Inflammation, Fibrosis and Tissue Repair. *Cells.* 2020;10.

8. Sutton MG, Sharpe N. Left ventricular remodeling after myocardial infarction: pathophysiology and therapy. *Circulation.* 2000;101:2981-2988.

9. Tillmanns J, Hoffmann D, Habbaba Y, et al. Fibroblast activation protein alpha expression identifies activated fibroblasts after myocardial infarction. *J Mol Cell Cardiol.* 2015;87:194-203.

10. Kratochwil C, Flechsig P, Lindner T, et al. (68)Ga-FAPI PET/CT: Tracer Uptake in 28 Different Kinds of Cancer. *J Nucl Med.* 2019;60:801-805.

11. Siebermair J, Kohler MI, Kupusovic J, et al. Cardiac fibroblast activation detected by Ga-68 FAPI PET imaging as a potential novel biomarker of cardiac injury/remodeling. *J Nucl Cardiol.* 2021;28:812-821.

12. Heckmann MB, Reinhardt F, Finke D, et al. Relationship Between Cardiac Fibroblast Activation Protein Activity by Positron Emission Tomography and Cardiovascular Disease. *Circ Cardiovasc Imaging.* 2020;13:e010628.

13. Varasteh Z, Mohanta S, Robu S, et al. Molecular Imaging of Fibroblast Activity After Myocardial Infarction Using a (68)Ga-Labeled Fibroblast Activation Protein Inhibitor, FAPI-04. *J Nucl Med.* 2019;60:1743-1749.

14. Langer LBN, Hess A, Korkmaz Z, et al. Molecular imaging of fibroblast activation protein after myocardial infarction using the novel radiotracer [(68)Ga]MHLL1. *Theranostics.* 2021;11:7755-7766.

15. Diekmann J, Koenig T, Zwadlo C, et al. Molecular Imaging Identifies Fibroblast Activation Beyond the Infarct Region After Acute Myocardial Infarction. *J Am Coll Cardiol.* 2021;77:1835-1837.

16. Kessler L, Kupusovic J, Ferdinandus J, et al. Visualization of Fibroblast Activation After Myocardial Infarction Using 68Ga-FAPI PET. *Clin Nucl Med.* 2021;46:807-813.

17. Notohamiprodjo S, Nekolla SG, Robu S, et al. Imaging of cardiac fibroblast activation in a patient after acute myocardial infarction using (68)Ga-FAPI-04. *J Nucl Cardiol.* 2021.

18. Gonzalez A, Schelbert EB, Diez J, Butler J. Myocardial Interstitial Fibrosis in Heart Failure: Biological and Translational Perspectives. *J Am Coll Cardiol.* 2018;71:1696-1706.

19. Loktev A, Lindner T, Burger EM, et al. Development of Fibroblast Activation Protein-Targeted Radiotracers with Improved Tumor Retention. *J Nucl Med.* 2019;60:1421-1429.

20. Goebel J, Seifert I, Nensa F, et al. Can Native T1 Mapping Differentiate between Healthy and Diffuse Diseased Myocardium in Clinical Routine Cardiac MR Imaging? *PLoS One.* 2016;11:e0155591.

21. Verhaert D, Thavendiranathan P, Giri S, et al. Direct T2 quantification of myocardial edema in acute ischemic injury. *JACC Cardiovasc Imaging.* 2011;4:269-278.

22. Rosmini S, Bulluck H, Captur G, et al. Myocardial native T1 and extracellular volume with healthy ageing and gender. *Eur Heart J Cardiovasc Imaging.* 2018;19:615-621.

23. Nagaraju CK, Dries E, Popovic N, et al. Global fibroblast activation throughout the left ventricle but localized fibrosis after myocardial infarction. *Sci Rep.* 2017;7:10801.

24. Salerno M, Kramer CM. Advances in parametric mapping with CMR imaging. *JACC Cardiovasc Imaging.* 2013;6:806-822.

25. Messroghli DR, Moon JC, Ferreira VM, et al. Clinical recommendations for cardiovascular magnetic resonance mapping of T1, T2, T2* and extracellular volume: A

consensus statement by the Society for Cardiovascular Magnetic Resonance (SCMR) endorsed by the European Association for Cardiovascular Imaging (EACVI). *J Cardiovasc Magn Reson.* 2017;19:75.

26. Humeres C, Frangogiannis NG. Fibroblasts in the Infarcted, Remodeling, and Failing Heart. *JACC Basic Transl Sci.* 2019;4:449-467.

27. Hess A, Thackeray JT, Wollert KC, Bengel FM. Radionuclide Image-Guided Repair of the Heart. *JACC Cardiovasc Imaging.* 2020;13:2415-2429.

28. Glasenapp A, Derlin K, Gutberlet M, et al. Molecular Imaging of Inflammation and Fibrosis in Pressure Overload Heart Failure. *Circ Res.* 2021;129:369-382.

29. Matsunari I, Schricke U, Bengel FM, et al. Extent of cardiac sympathetic neuronal damage is determined by the area of ischemia in patients with acute coronary syndromes. *Circulation.* 2000;101:2579-2585.

30. Beijnink CWH, van der Hoeven NW, Konijnenberg LSF, et al. Cardiac MRI to Visualize Myocardial Damage after ST-Segment Elevation Myocardial Infarction: A Review of Its Histologic Validation. *Radiology.* 2021;301:4-18.

31. Gholap NN, Achana FA, Davies MJ, Ray KK, Gray L, Khunti K. Long-term mortality after acute myocardial infarction among individuals with and without diabetes: A systematic review and meta-analysis of studies in the post-reperfusion era. *Diabetes Obes Metab.* 2017;19:364-374.

32. Johansson S, Rosengren A, Young K, Jennings E. Mortality and morbidity trends after the first year in survivors of acute myocardial infarction: a systematic review. *BMC Cardiovasc Disord.* 2017;17:53.

33. Regan TJ, Lyons MM, Ahmed SS, et al. Evidence for cardiomyopathy in familial diabetes mellitus. *J Clin Invest.* 1977;60:884-899.

34. Russo I, Frangogiannis NG. Diabetes-associated cardiac fibrosis: Cellular effectors, molecular mechanisms and therapeutic opportunities. *J Mol Cell Cardiol.* 2016;90:84-93.

35. Werner RA, Koenig T, Diekmann J, et al. CXCR4-Targeted Imaging of Post-Infarct Myocardial Tissue Inflammation: Prognostic Value After Reperfused Myocardial Infarction. *JACC Cardiovasc Imaging.* 2021.

36. Abgral R, Dweck MR, Trivieri MG, et al. Clinical Utility of Combined FDG-PET/MR to Assess Myocardial Disease. *JACC Cardiovasc Imaging.* 2017;10:594-597.

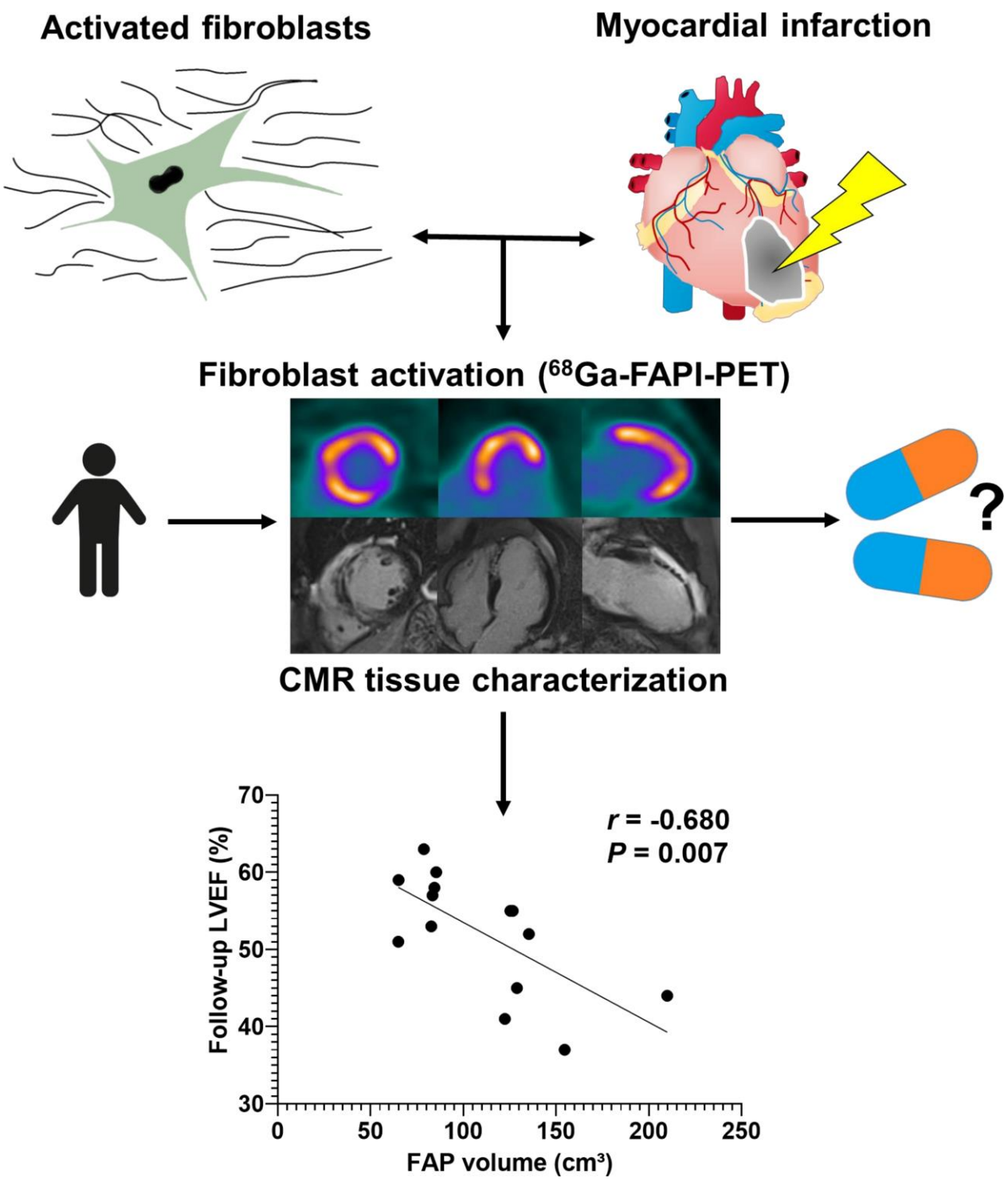

Graphical Abstract

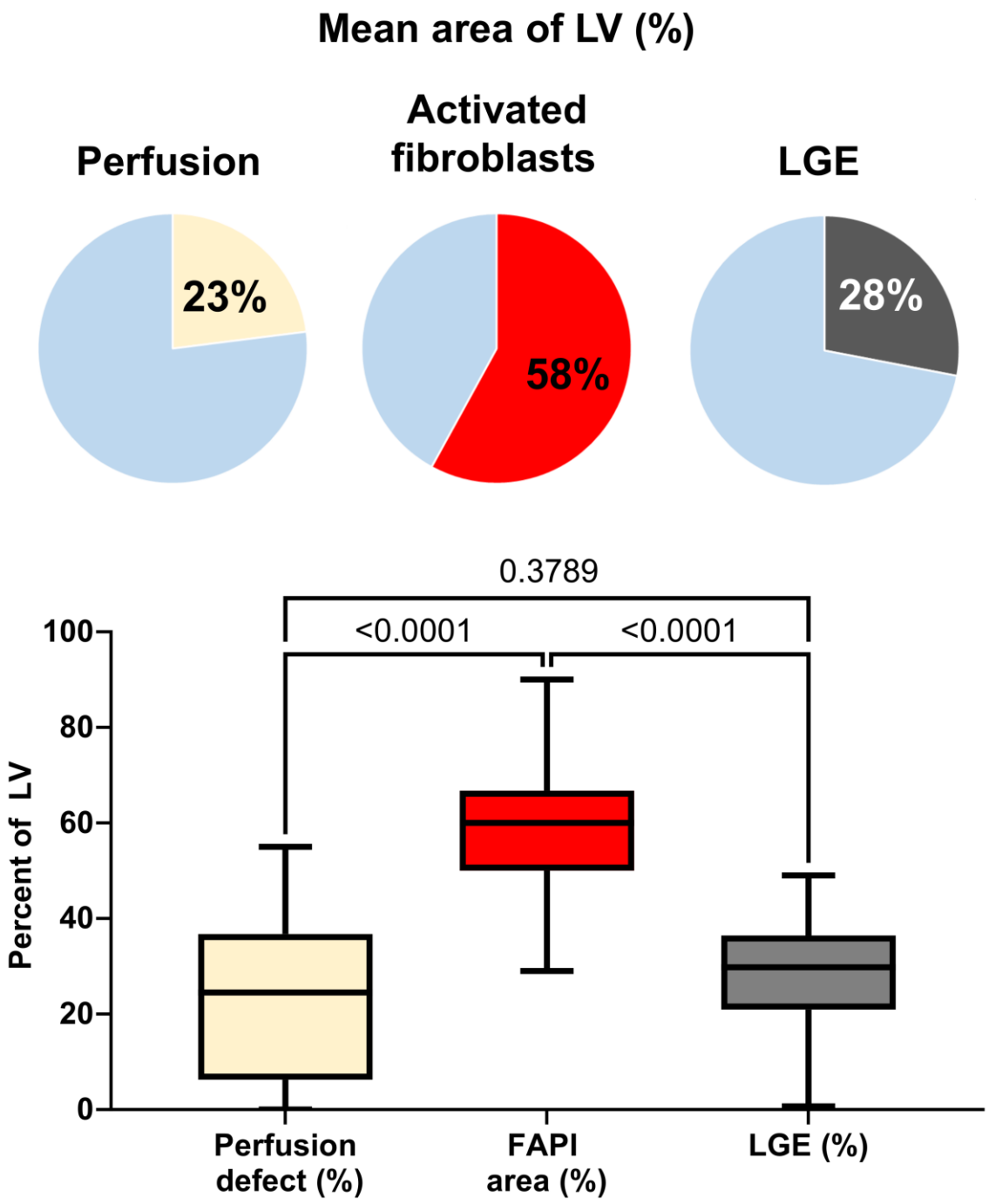

Figure 1: Boxplot analysis (mean, min-max) of perfusion defect size (yellow), activated fibroblasts (red) and LGE (grey) in the entire patient group, expressed as percent of LV.

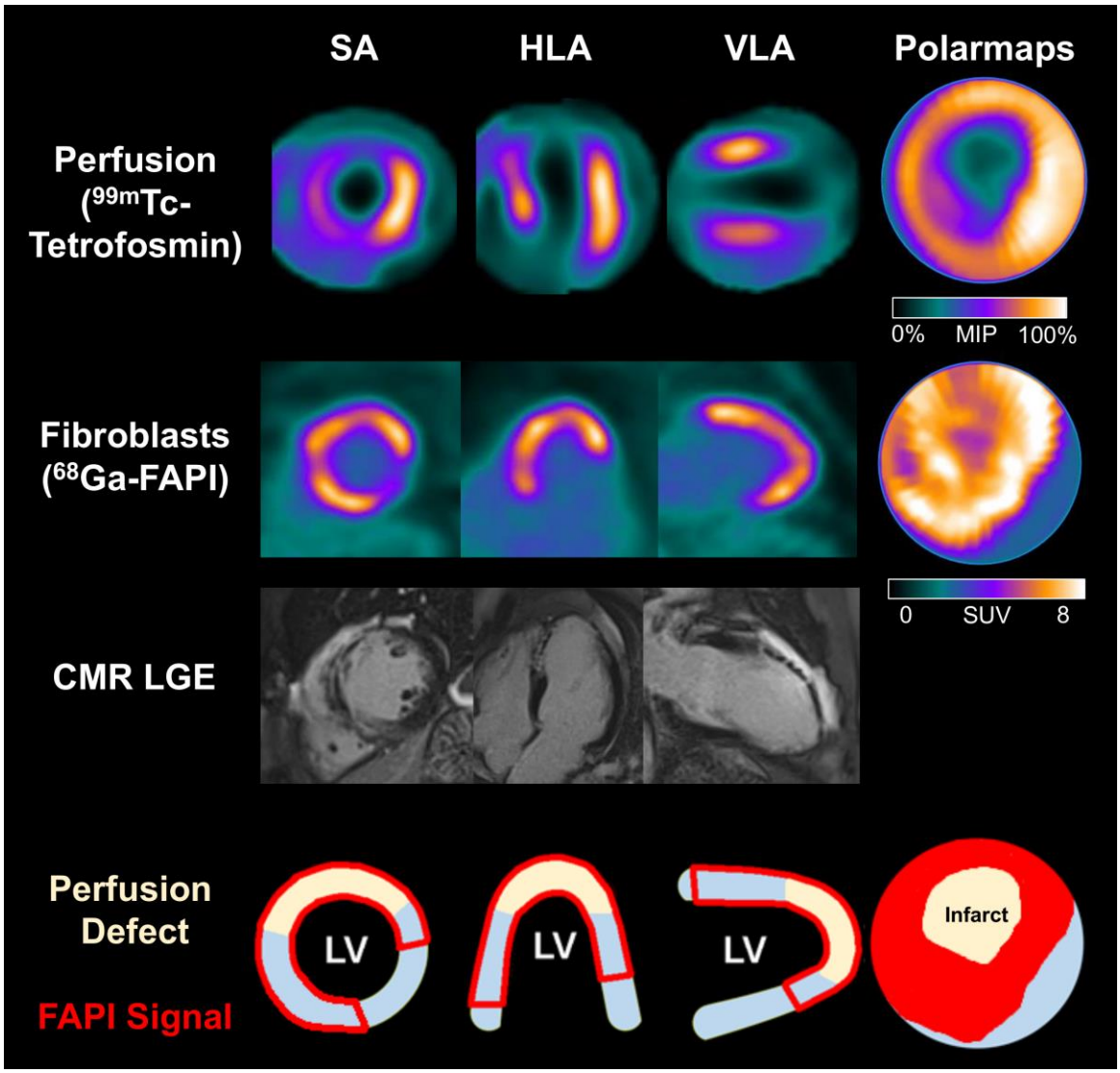

Figure 2: ^{68}Ga-FAPI-46 PET signal exceeds the infarct region after acute myocardial infarction (AMI). Depicted are: Myocardial perfusion images using ^{99m}Tc-tetrofosmin at rest (first row), ^{68}Ga-FAPI PET (second row), late gadolinium enhancement (LGE) from cardiac magnetic resonance (third row) and schematic drawings of the left ventricle (fourth row). Area of fibroblast activation exceeds infarct area and LGE signal, most common type of myocardial FAP-distribution. SA, short axis; HLA, horizontal long axis; VLA, vertical long axis; SPECT, single photon emission computed tomography; PET, positron emission tomography; SUV, standardized uptake value; CMR, cardiac magnetic resonance imaging; LGE, gadolinium contrast late enhancement; LV, left ventricle.

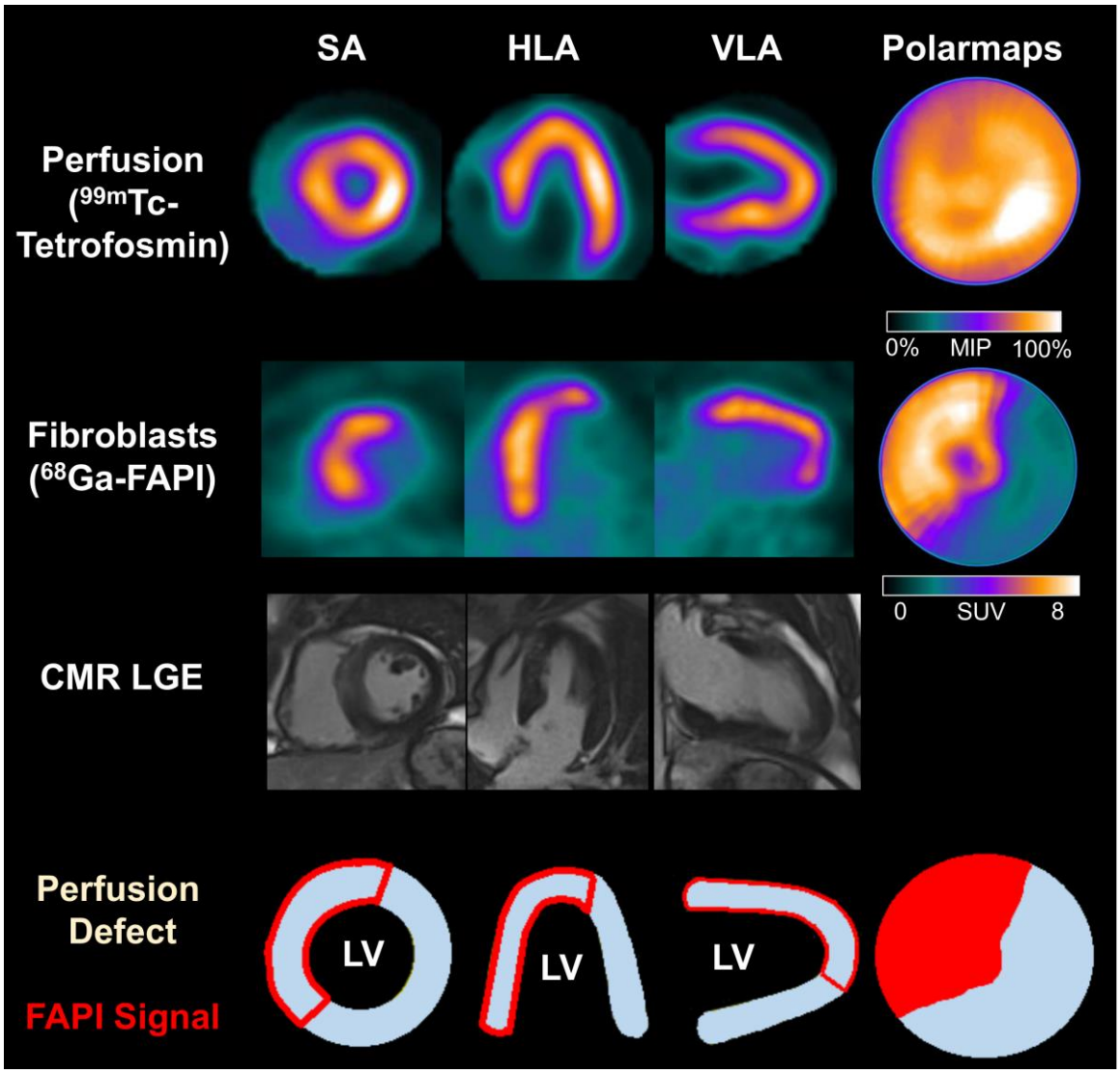

Figure 3: No relevant perfusion defect after AMI due to complete reperfusion, no significant LGE but a large area of fibroblast activation.

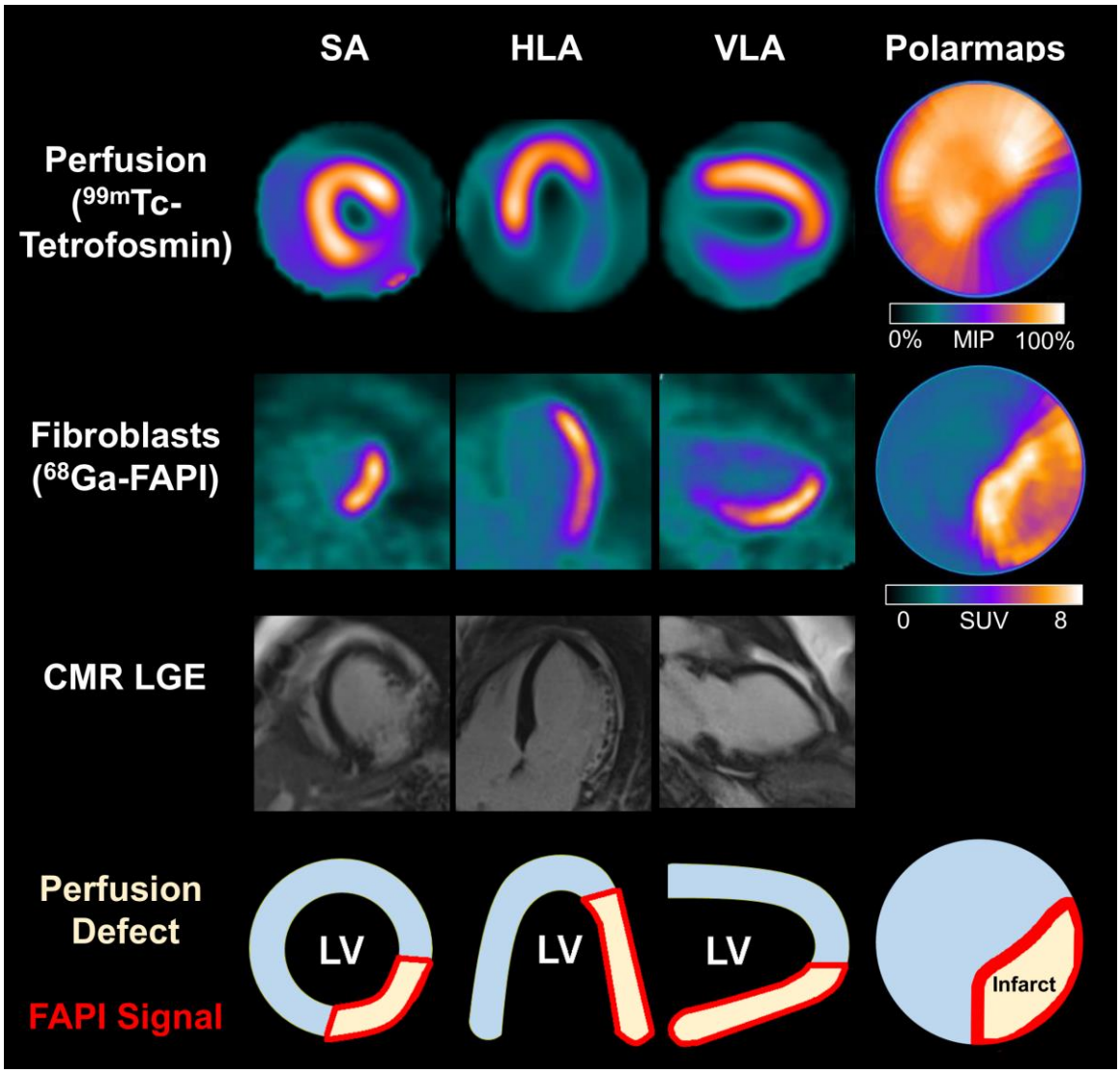

Figure 4: Fibroblast activation is only marginally exceeding the infarct region.

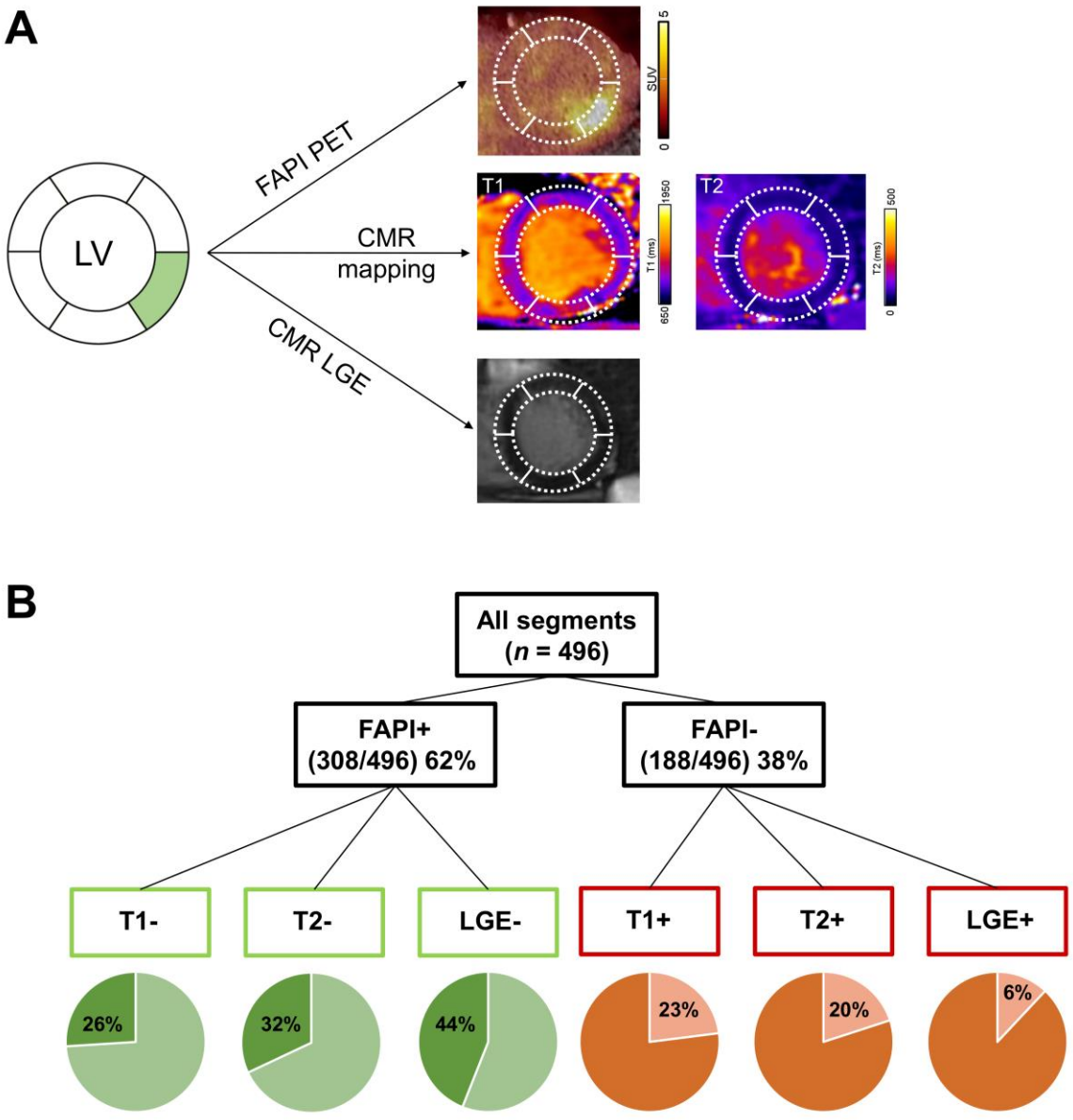

Figure 5: (A) Patient example with a FAP +, T1 -, T2 - and LGE – segment. (B) Segmental comparison of myocardial ^{68}Ga-FAPI-46 distribution, native T1 and T2 mapping and late gadolinium enhancement (LGE) from cardiac magnetic resonance imaging, using a 16-segment model (apex excluded) in 31 AMI patients with complete datasets, resulting in a total of n=496 segments.

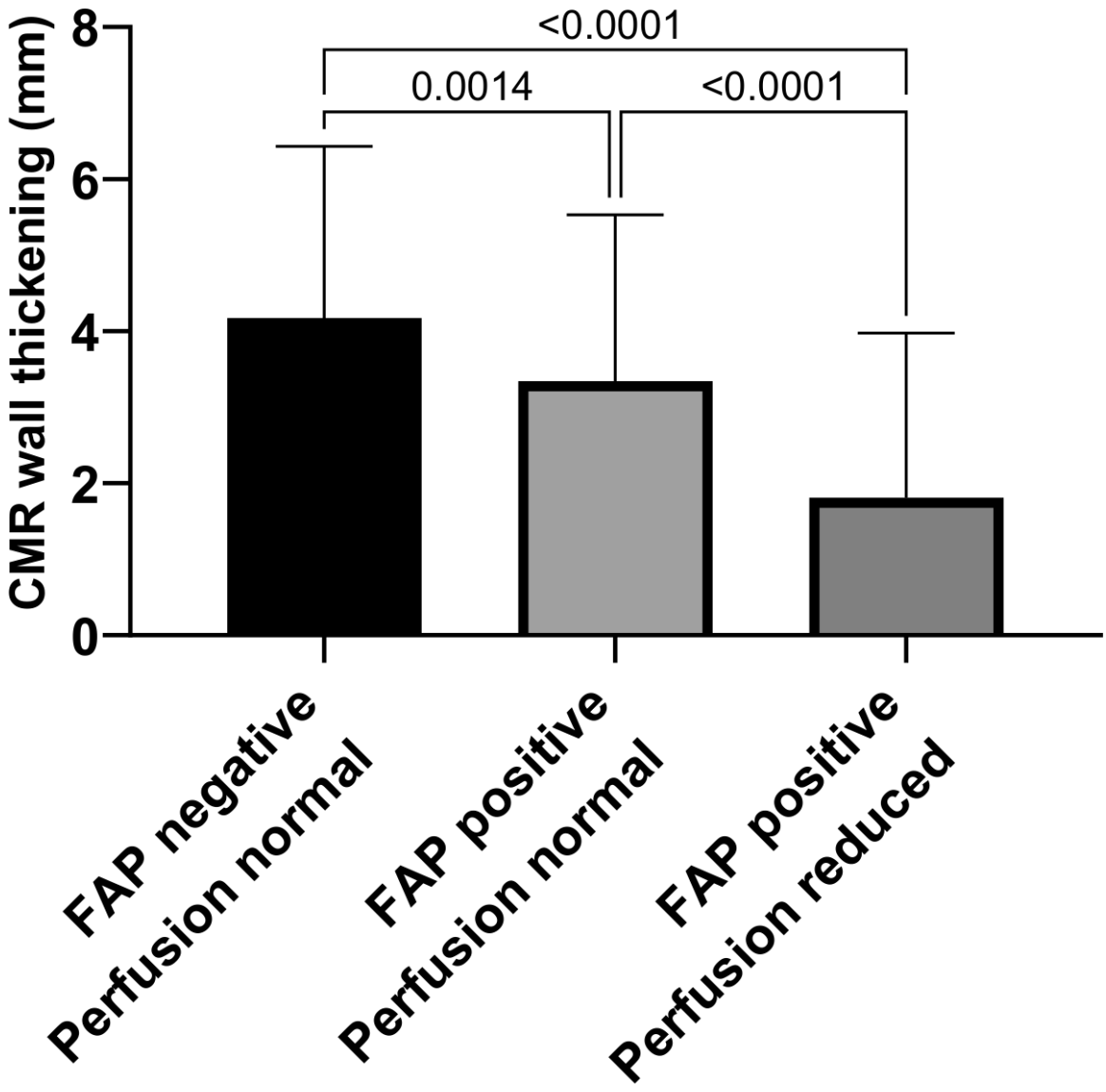

Figure 6: Three groups were built for analysis of wall thickening and contractility: 1. FAP- and normally perfused segments representing remote myocardium, 2. FAP+ but normally perfused segments representing border zone and FAP+ segments with reduced perfusion representing core infarct zone. Wall thickening was significantly impaired in all FAP+ segments with or without reduced perfusion (infarct and border zone).

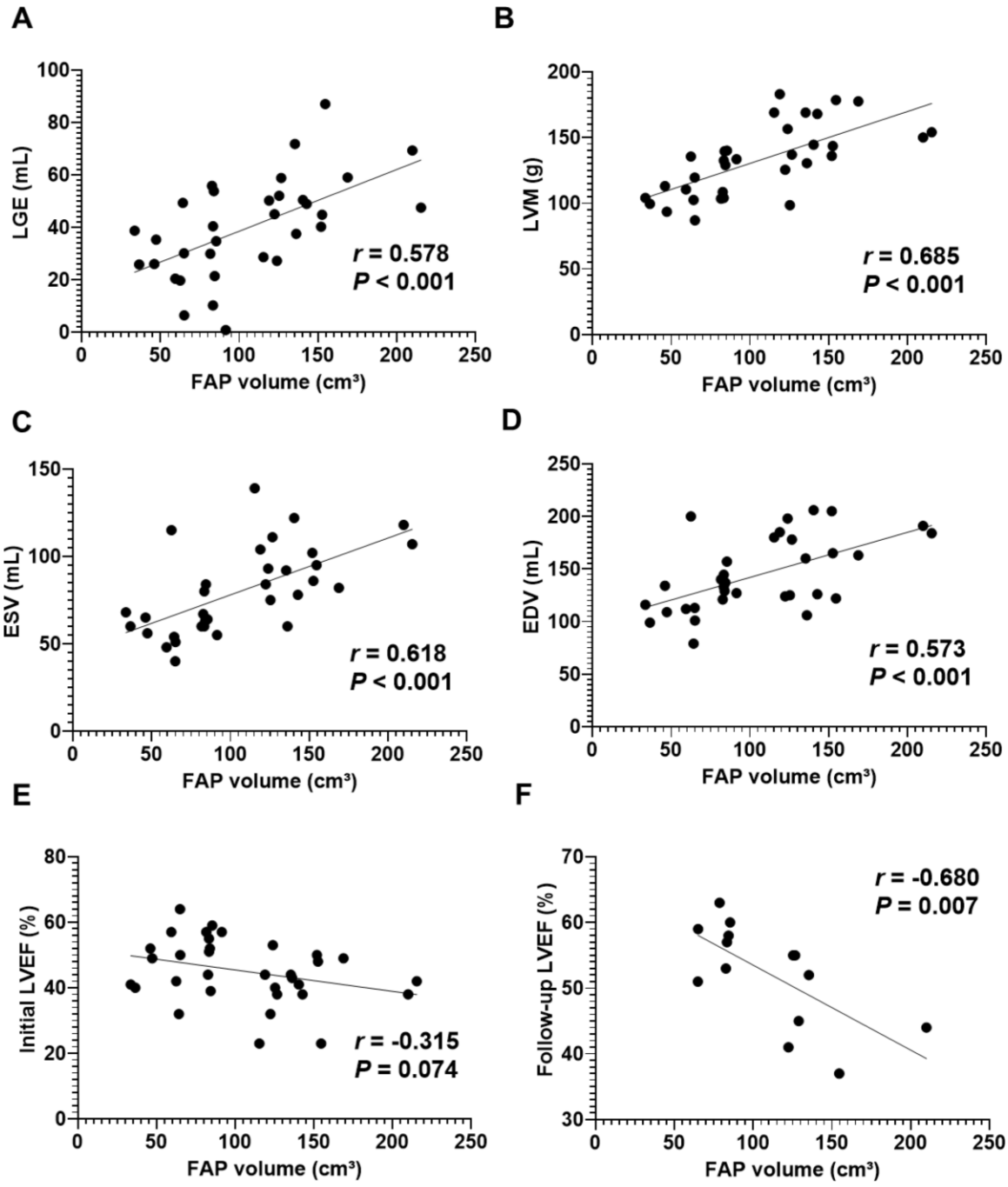

Figure 7: Global myocardial FAP volume early after acute myocardial infarction correlates with synchronously measured markers of cardiac geometry and function from cardiac magnetic resonance: (A) volume of late gadolinium enhancement (LGE; ml); (B) left ventricular mass (LVM; g); (C) endsystolic and (D) enddiastolic volume (ESV, EDV; ml). A non-significant trend to correlation was found with left ventricular ejection fraction (LVEF) at baseline (E) while a significant correlation with follow-up LVEF was detected (F).

Table 1. Patient Characteristics

Variable		*all patients (n=35)*
Age (years)		57±11
Sex (n (%))	Female	5/35 (14.3)
	Male	30/35 (85.7)
Height (cm)		178±7
Weight (kg)		86.8±15.8
Cardiovascular risk factors (n (%))	Diabetes	11/35 (31.4)
	Arterial hypertension	19/35 (54.3)
	Dyslipidemia	25/35 (71.4)
	Obesity (BMI >30 kg/m²)	9/35 (25.7)
	Smoking	21/35 (60.0)
Culprit Vessel (n (%))	LAD	24/35 (68.6)
	LCX	3/35 (8.6)
	RCA	8/35 (22.9)
Symptom to wire time (min)		234±190
Peak creatine kinase (CK, U/l)		3416±3104
Peak c-reactive protein (CRP, mg/l)		42.6±53.2
Peak leukocyte count (1000/mm³)		14.4±4.4
Peak creatinine (mg/dl)		97.1±20.7
Medication at PET (n (%))	ASS	32/35 (91.4)
	P2Y12-antagonists	35/35 (100)
	OAK	3/35 (8.5)
	Statins	35/35 (100)
	Beta-blockers	33/35 (94.3)
	Non-insulin glucose-lowering drugs	11/35 (31.4)
	Insulin	2/35 (5.7)
	ACE-inhibitors	22/35 (62.9)
	ATII-blockers	13/35 (37.1)

MI, myocardial infarction; LAD, left anterior descending coronary artery; LCX, left circumflex coronary artery; RCA, right coronary artery; PET, positron emission tomography; OAK, oral anticoagulation; ACE, angiotensin converting enzyme; ATII, angiotensin 2.

Table 2. Cardiac Magnetic Resonance Imaging

Variable	*all patients (n=33)*	*range*
Global function parameters		
LVM (g)	132.6±27.4	87-183
EDV (ml)	144.5±35.5	79-206
ESV (ml)	79.9±25.0	40-139
SV (ml)	64.7±20.1	25-105
LVEF (%)	45.1±9.6	23-64
LGE (ml)	39.9±19.0	0.8-87
LGE (% of ventricle)	28.3±11.2	0.7-49
MO (%)	1.0±1.2	0-5.2

LVM, left ventricular mass; EDV, enddiastolic volume; ESV, endsystolic volume; SV, stroke volume; LVEF, left ventricular ejection fraction; LGE, late gadolinium enhancement; MO, microvascular obstruction

Table 3. Radionuclide Imaging

Variable	*all patients (n=35)*	*range*	*CMR available (n=33)*	*range*
Perfusion defect (SPECT % of polar map)	23.2±17.4	0-55	23.6±17.4	0-55
PET signal (^{68}Ga-FAPI-46 SUV_{peak})				
Spleen	1.43±0.40	0.96-2.61	1.43±0.41	0.96-2.61
Liver	1.50±0.47	0.82-2.93	1.48±0.47	0.82-2.93
Bone marrow	1.05±0.29	0.61-2.04	1.05±0.29	0.61-2.04
Lungs	0.82±0.32	0.34-2.17	0.81±0.33	0.34-2.17
Blood pool (left atrium)	1.97±0.40	1.32-3.21	1.97±0.40	1.32-3.21
Remote myocardium	1.41±0.38	0.91-2.84	1.41±0.39	0.91-2.84
Infarct	6.41±1.53	3.52-10.60	6.54±1.46	4.24-10.60
Area of FAP-upregulation (% of polar map)	58.0±15.4	29-90	57.7±15.8	29-90
Volume of FAP-signal (cm^3)	105.8±45.6	33.6-215.4	105.9±46.6	33.6 -215.4

PET, positron emission tomogaphy; MBq, megabequerel; Ga, gallium; FAPI, fibroblast activation protein inhibitor; SUV, standardized uptake value, SPECT, single photon emission computed tomography